# Magnetism-correlated high-temperature martensitic phase transition in ductile Co₂NiT ($T$ = Sc, Ti, V, Cr, Y, Zr, Nb, Mo, Hf, Ta, and W) all-$d$-metal Heusler compounds

Guijiang Li ,[*] Lei Xu, and Zhenhua Cao

*College of Materials Science and Engineering, Nanjing Tech University, Nanjing 211816, People's Republic of China*

To explore martensitic phase transition materials with outstanding performance, phase stability, magnetism, and ductility of all-$d$-metal Heusler compounds Co₂NiT ($T = t$ transition metal) were symmetrically investigated by density functional theory calculations. Different from $p$-$d$ covalent hybridization-dominated conventional Heusler compounds, all-$d$-metal Heusler compounds, i.e., Co₂NiT with transition metal atoms Ti, V, Cr, Nb, Mo, Ta, and W, prefer $L2_1$-type structure rather than Hg₂CuTi-type structure. Moreover, inherent atomic radii become the decisive factor when determining the lattice sizes. Owing to the Kohn anomaly, high-temperature martensitic phase transitions can occur in Co₂NiT compounds, which was also confirmed by the peak-and-valley-characterized density of states near the Fermi level and deep softening of transverse acoustic phonon modes as well as negative tetragonal shear elastic constant. Importantly, compared with conventional Heusler compounds, the replacement of nondirectional $d$-$d$ metallic bonding for $p$-$d$ covalent hybridization boosts more uniform distribution of electrons and enhances metallicity, which consequently improves the ductility of Co₂NiT compounds. Comparatively, herein, it was found that, although magnetism is not the necessary condition for the occurrence of martensitic phase transition, the loss of magnetism can destabilize the cubic structure. Therefore, tuning magnetism can serve as another effective way to adjust martensitic phase transition in all-$d$-metal Heusler compounds. The small volume change ratio during martensitic phase transition in Co₂NiTi and Co₂NiV compounds endows them with more extensive application prospects. Hopefully, this paper can help better understand the mechanism of martensitic phase transition and its correlation to magnetism and origin of improved ductility in all-$d$-metal Heusler compounds Co₂NiT, which may accelerate the exploration of excellent high-temperature martensitic phase transition materials.

## I. INTRODUCTION

Energy-efficient and environmentally friendly solid-state refrigeration based on phase transition has been considered the most promising alternative to the conventional vapor-compression cooling technology in the context of global carbon neutralization [1–3]. For the practical realization of the application of clean solid-state refrigeration, the essential prerequisite involves the development of phase transition materials with outstanding performance. Previously, significant productive efforts have been devoted to exploring high-performance phase transition materials with high refrigeration capacity and service ability [4,5]. Among all the potential candidate phase transition materials used for refrigeration applications, $X_2YZ$-type ($X/Y$ = transition metal, $Z$ = main − group element) Heusler compounds are more attractive due to their rich candidate material systems, tunable phase transition temperature and hysteresis, quick response to multiple fields, and higher multiple-caloric effects [6,7]. However, in $X_2YZ$-type conventional Heusler compounds, a stronger $p$-$d$ covalent hybridization exists between electrons in the $p$ orbital of main-group elements and $d$ orbital of transition metals. This covalent hybridization results in

brittleness, which is consequently a major obstacle to restrict the application of Heusler compounds. Notably, the brittleness originates from $p$-$d$ covalent hybridization; therefore, the replacement of $d$-$d$ metallic bonding for $p$-$d$ covalent hybridization could help to overcome the brittleness. Thus, by substituting transition metals for main-group elements, the all-$d$-metal Heusler compounds were designed and explored. Owing to the fundamental transition of interatomic bonding style from directional $p$-$d$ covalent hybridization in convention Heusler compounds to $d$-$d$ metallic bonding, significant improvement of mechanical properties and typical martensitic phase transition have been theoretically and experimentally observed in all-$d$-metal Heusler compounds [8–12], making them more attractive from the perspective of not only industrial application but also fundamental research. Noteworthy, the concept of ductility as well as its physical mechanism is unique to all-$d$-metal Heusler compounds. Furthermore, largely different from conventional Heusler compounds, the currently available observations show that all transition metal atoms in all-$d$-metal Heusler compounds can contribute to the magnetic moment [13,14]. Under these circumstances, magnetism becomes an indispensable factor when discussing martensitic phase transition in all-$d$-metal Heusler compounds, particularly in strong ferromagnetic (FM) compounds. To reveal the role of magnetism on martensitic phase transition, suitable all-$d$-metal compound systems

─────────
[*]guijiangli@njtech.edu.cn
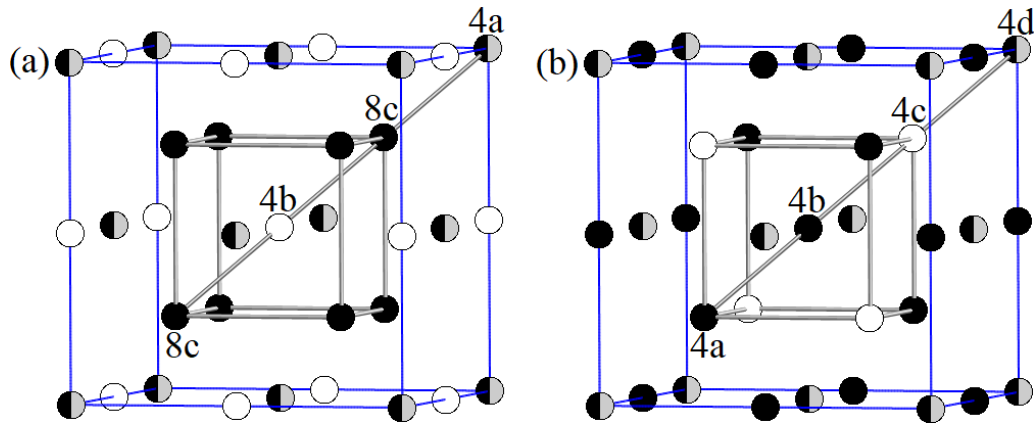
FIG. 1. (a) $Cu_2MnAl$-type structure (space group $Fm\bar{3}m$, No. 225), in which the Wyckoff sites of $8c$, $4b$, and $4a$ are (0.25,0.25,0.25)/ (0.75,0.75,0.75), (0.5,0.5,0.5), and (0,0,0), respectively; and (b) $Hg_2CuTi$-type structure (space group $F\bar{4}3m$, No. 216), in which the Wyckoff sites of $4a$, $4b$, $4c$, and $4d$ are (0.25,0.25,0.25), (0.5,0.5,0.5), (0.75,0.75,0.75), and (0,0,0), respectively.

with diversified magnetic exchange coupling styles, i.e., FM, ferrimagnetic (FIM), and nonmagnetic (NM) states, are necessary. Thus, the main objective of this paper was to explore all-$d$-metal Heusler compounds with typical martensitic phase transition and outstanding comprehensive performance for future applications and reveal the related physical mechanism for martensitic phase transition and ductility. Based on these all-$d$-metal Heusler compounds, the correlation between magnetism and martensitic phase transition was further addressed.

Related literature investigations indicate that very few $Co_2NiT$'s ($T$ = Sc, Ti, V, Cr, Y, Zr, Nb, Mo, Hf, Ta, and W) have been shown as cubic all-$d$-metal Heusler compounds experimentally. Although a compound with the composition of $Co_2NiV$ was synthesized previously, the reported structure was trigonal [15]. Thus, the $Co_2NiT$ all-$d$-metal Heusler compounds are unique to the Heusler family. Moreover, current theoretical calculations indicate that $Co_2NiT$ all-$d$-metal Heusler compounds show the possibility of martensitic phase transition and possess variable magnetic states. Thus, $Co_2NiT$ all-$d$-metal Heusler compounds could be considered an ideal system and consequently provide a platform to systematically investigating martensitic phase transition, magnetism, and correlations between them. Moreover, the mechanism of martensitic phase transition and physical origin of improved ductility are discussed in detail in this paper. Hopefully, this paper can help to explore more excellent phase transition materials for solid-state refrigeration with outstanding mechanical properties from both experimental and theoretical perspectives.

This paper is organized as follows: The calculation details are listed in Sec. II. The results and discussion are presented in Sec. III. First, determination of the stable structures within the scope of the Heusler family is presented. Then based on the calculated elastic properties, electronic structure, lattice dynamics, and magnetism, the martensitic phase transition, magnetism, and their correlations and improved ductility are discussed. Finally, the quasivolume-preserving characteristic of martensitic phase transition is revealed. The conclusions of this paper are summarized in Sec. IV.

## II. CALCULATIONS METHODS

Based on the atomic preferential occupation rule in conventional full Heusler compounds [16] and knowledge about all-$d$-metal Heusler compounds [9–14], both $L2_1$- and $Hg_2CuTi$-type structures were initially considered herein for all-$d$-metal Heusler compounds $Co_2NiT$. They are shown in Figs. 1(a) and 1(b), respectively. Based on geometrical optimization, the preferential crystal structures were determined for $Co_2NiT$ compounds. Based on the preferential structures, the first-principles calculations were carried out.

In this paper, the structural parameters, elastic properties, electronic structure, lattice dynamics, and magnetism of all-$d$-metal Heusler compounds $Co_2NiT$ were investigated by density functional theory (DFT). The calculations were carried out by using CASTEP code via the pseudopotential method. Similar methods to those reported in the literature were used to calculate elastic constants [17]. During calculations, the energy convergence criterion was set to $1\times10^{-6}$ eV atom$^{-1}$. The density plane-wave cutoff was 500 eV. The ultrasoft pseudopotential was adopted to describe the interactions between the atomic core and the valence electrons [18]. During the calculations by CASTEP, the exchange-correlation energy of electrons was dealt with by GGA-PBE [19]. The size of supercell was 27 times that of the primitive cell used in the calculation of the phonon properties. A Monkhorst-Pack phonon $q$-vector grid of $8\times8\times8$ was adopted for the calculation of phonon dispersions and phonon density of states (DOS). A Monkhorst-Pack $k$-point grid of $15\times15\times15$ was used for the electronic properties of cubic all-$d$-metal Heusler compounds $Co_2NiT$. The adopted $k$-point meshes in the tetragonal structures were closely dependent on the $c/a$ ratios.

When dealing with disordered B2- and A2-type structures, the random occupation of atoms in all-$d$-metal Heusler compounds $Co_2NiT$ was explored by using the Korringa-Kohn-Rostoker coherent potential approximation [20,21]. The energy differences between high-ordered $L2_1$- and $Hg_2CuTi$-type structures and disordered B2- and A2-type structures were calculated to determine the stable structures within the scope of Heusler structures.
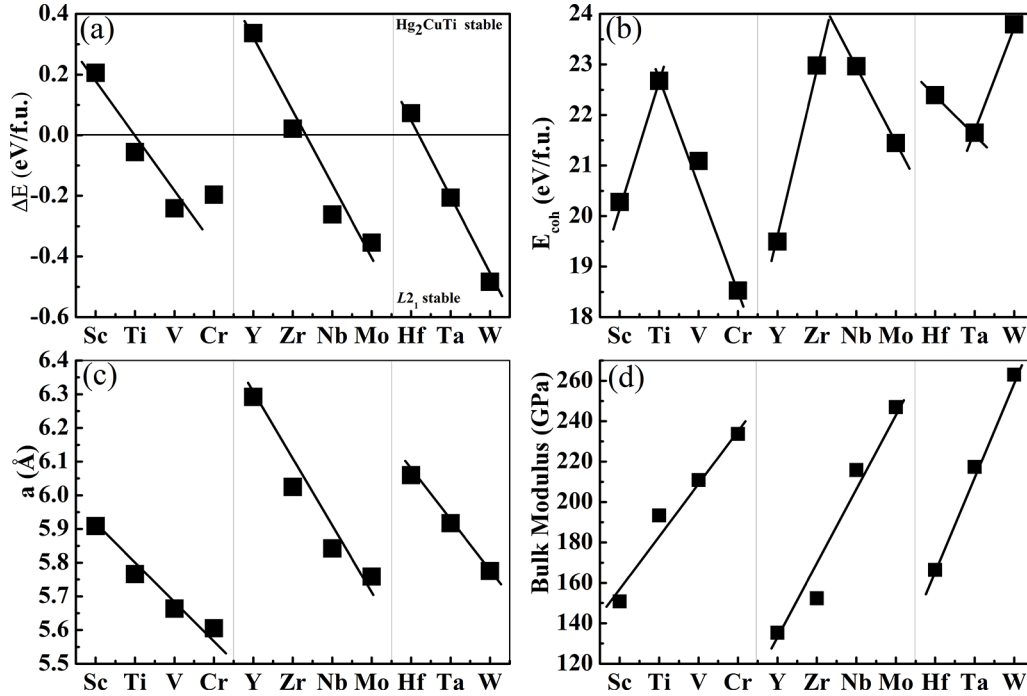
FIG. 2. Ground state structural parameters of $Co_2NiT$ ($T$ = Sc, Ti, V, Cr, Y, Zr, Nb, Mo, Hf, Ta, and W) compounds at theoretical equilibrium states: (a) The $\Delta E$ (in eV f.u.$^{-1}$) between the $Cu_2MnAl$-type (i.e., $L2_1$-type) and $Hg_2CuTi$-type structures of $Co_2NiT$. The line in figure is to guide the eye to separate the $Hg_2CuTi$- and $Cu_2MnAl$-type structures, which corresponds to the positive and negative $\Delta E$ range, respectively. (b) Cohesive energies $E_{coh}$ (in eV f.u.$^{-1}$) of $Co_2NiT$. (c) Lattice parameter a (in Å) of $Co_2NiT$. (d) Bulk modulus $B$ (in GPa) of $Co_2NiT$.

## III. RESULTS AND DISCUSSION

### A. Structural information at the ground states

Following the atomic preferential occupation rule in conventional $X_2YZ$-type Heusler compounds [16], $Co_2NiT$ compounds could acquire $Hg_2CuTi$-type structures. Based on previous studies on all-$d$-metal Heusler compounds, some all-$d$-metal Heusler compounds, particularly with late transition metals, do not obey the atomic preferential occupation rule in conventional Heusler compounds [12,13,22]. Thus, both $L2_1$- and $Hg_2CuTi$-type structures were simultaneously considered in $Co_2NiT$ compounds. The calculated crystal structure parameters are presented in Fig. 2. The preferred crystal structures of $Co_2NiT$ compounds were determined by energy difference ($\Delta E$) between the $L2_1$- and $Hg_2CuTi$-type structures. Within the scope of Heusler-type structures, negative $\Delta E$ indicates that the $L2_1$-type structure is relatively stable. Otherwise, the $Hg_2CuTi$-type structure is stable. Figure 2(a) exhibits that the $Co_2NiT$ compounds with early transition metals such as Sc, Y, Zr, and Hf show positive $\Delta E$. In contrast, the values of $Co_2NiT$ compounds with late transition metals on the right of the periodic table are all negative. This result indicates that $Co_2NiT$ ($T$ = Ti, V, Cr, Nb, Mo, Ta, and W) compounds prefer the $L2_1$-type structures. The two Co atoms equally occupy the $8c$ sites. Moreover, Ni and transition metal atoms ($T$ = Ti, V, Cr, Nb, Mo, Ta, and W) reside in $4b$ and $4a$ sites, respectively. This atomic configuration style is contrary to the generalized adopted atomic preferential occupation rule in conventional Heusler compounds. Similar atomic occupation behaviors were also observed in other all-$d$-metal Heusler compounds with late transition metals

[12,13,22]. The remaining $Co_2NiT$ compounds ($T$ = Sc, Y, Zr, and Hf) explored in this paper preferred to remain in $Hg_2CuTi$-type structures rather than the $L2_1$-type structures. The two Co atoms occupy $4a$ and $4b$ sites, respectively. Moreover, Ni and transition metals are located in $4c$ and $4d$ sites.

In solids, cohesive energy can be used to describe the strength of interatomic bonding and thermodynamic stability of materials. Theoretically, the cohesive energy of $Co_2NiT$ compounds was obtained in this paper by the function of $E_{coh} = (2E_{Co}^{iso} + E_{Ni}^{iso} + E_T^{iso}) - E_{Co_2NiT}^{Total}$, where $E_{Co}^{iso}$, $E_{Ni}^{iso}$, and $E_T^{iso}$ are isolated atomic energy of Co, Ni, and $T$ atoms, respectively. Here, $E_{Co_2NiT}^{Total}$ denotes the total energy of $Co_2NiT$ compounds. In this paper, the theoretical cohesive energy values of $Co_2NiT$ compounds shown in Fig. 2(b) range from 18.5 to 23.8 eV f.u.$^{-1}$. These high values indicate strong chemical bonding in $Co_2NiT$ compounds, which can be compared with those in stable Heusler compounds [12,17]. Moreover, these large $E_{coh}$ values also indicate that $Co_2NiT$ compounds are thermodynamically stable at their specific structures. For $Co_2NiV$, the reported crystal structure in the experimental literature [15] and Materials Project database [23] belongs to the trigonal crystal system rather than the $L2_1$-type structure. For trigonal $Co_2NiV$, the calculated cohesive energy is 21.8 eV f.u.$^{-1}$, which is slightly higher than that of $L2_1$-type $Co_2NiV$ (21.1 eV f.u.$^{-1}$). Comparatively, $L2_1$-type $Co_2NiV$ is metastable. Except for the crystal structure and lattice parameters, information about constituent phases at high temperature is lacking in the literature. The similar cohesive values of trigonal and $L2_1$-type $Co_2NiV$ may indicate the possibility of coexistence of these two phases at high temperature. Inspired
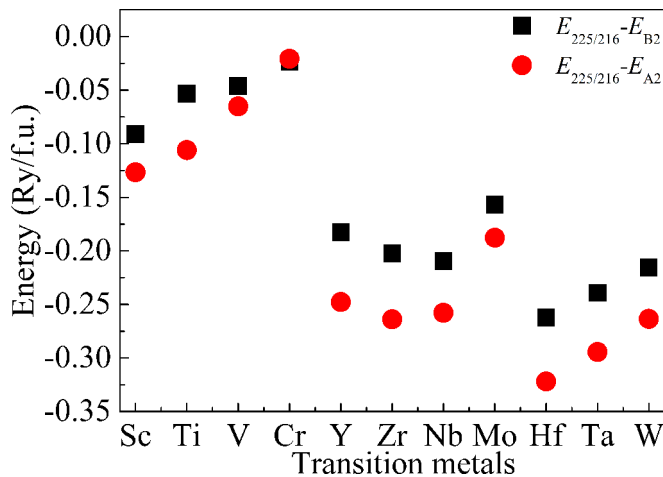
FIG. 3. The energy difference between the ordered $L2_1$- or $Hg_2CuTi$-type structures, and disordered B2- and A2-type structures in all-$d$-metal Heusler compounds $Co_2NiT$ ($T$ = Sc, Ti, V, Cr, Y, Zr, Nb, Mo, Hf, Ta, and W).

by a previous study on $Ni_2FeGa$ [24], the metastable $Co_2NiV$ Heusler compound could be obtained by selecting suitable preparation methods and heat treatments. Thus, the possibility of experimental synthesis of $L2_1$-type $Co_2NiV$ and the remaining $Co_2NiT$ compounds deserves further confirmation.

The atomic disordered occupation has been frequently mentioned in Heusler compounds, which could impose important effects on the physical properties. When atomic disorder occupation occurs, two possible disordered structures, i.e., B2- and A2-type structures, are typically observed [25]. In $X_2YZ$-type Heusler compounds, when $Y$ and $Z$ atoms randomly occupy the $4a$ and $4b$ sites in $L2_1$-type structures and $4b$ and $4d$ sites in $Hg_2CuTi$-type structures, the B2-type structure is obtained. In A2-type structures, the four $X$, $Y$, and $Z$ atoms randomly occupy all sites of Heusler compounds. To determine the stable atomic configuration within the scope of Heusler-type crystal structures, the total energy differences between ordered $L2_1$- or $Hg_2CuTi$-type structures and disordered B2- and A2-type structures were calculated. The corresponding results are presented in Fig. 3. Obviously, all the energy difference values are negative, indicating that the ordered cubic structures are relatively stable. Comparatively, when changing from B2- to A2-type structure, the energy differences become much smaller. The increase in atomic disorder level is responsible for this enhanced energy difference. The higher the atomic disorder level, the less stable the material. In contrast, the ordered cubic structures are more stable and could be considered the ground-state structures within the scope of the Heusler family.

Under the abovementioned atomic preferential configuration, the lattice sizes of $Co_2NiT$ at ground states were obtained by geometry optimization and shown in Fig. 2(c). For $T$ atoms in the same period, the lattice parameters of $Co_2NiT$ decrease with the increase of the number of valence electrons. In most Heusler compounds, the bulk modulus follows the general trend that a larger bulk modulus commonly corresponds to a smaller lattice size [12]. Thus, the dependence of the bulk modulus on specific transition metal

atoms shows inverse change behaviors to those of lattice parameters, as shown in Fig. 2(d). Currently, the difference of lattice sizes among all-$d$-metal Heusler compounds originates from the atomic radii of transition metals. For atoms in the same period, their atomic radii decrease with the increase of valence electrons from left to right in the periodic table. The distribution of atomic size is the same as the change of dependency of lattice parameter on specific transition metal atoms in $Co_2NiT$ compounds [see Fig. 2(c)]. Thus, the inherent atomic size was considered the determining factor on lattice parameters in all-$d$-metal Heusler compounds. However, in conventional Heusler compounds, other than atomic radii, the $p$-$d$ interatomic orbital hybridization between the first-nearest-neighbor (1nn) main-group elements and transition metals is also crucially important when determining the lattice size. In main-group-element-rich compounds, the stronger covalent hybridization level can shrink lattice sizes, resulting in kink behavior in the lattice-parameter-dependent main-group-element composition curve [26–28]. Commonly, the inherent atomic radius and the interatomic $p$-$d$ hybridization codetermine the lattice size of conventional Heusler compounds. However, in all-$d$-metal Heusler compounds, covalent hybridization weakens due to the full replacement of transition metals for main-group elements, and consequently, it no longer dominates the lattice size, which will be verified in the next section.

### B. Elastic-parameter-based determination of phase stability and ductile properties

Based on the abovementioned preferential crystal structure, elastic constants and their derived parameters of $Co_2NiT$ compounds were calculated and summarized in Table SI in the Supplemental Material [29]. For comparative analysis, elastic parameters of conventional $Co_2NiGa$ are also listed herein. The high consistency between current data of $Co_2NiGa$ and previous results [30,31] strongly indicates that current calculations are valid and suitable to deal with $Co_2NiT$ Heusler compounds.

For cubic compounds, the three independent elastic constants are $C_{11}$, $C_{12}$, and $C_{44}$, respectively. The sufficient and necessary condition of mechanical stability is given as $C_{11} > 0$, $C_{44} > 0$, $C_{11} + 2C_{12} > 0$, and $C' = \frac{C_{11} - C_{12}}{2} > 0$ [32]. All these $Co_2NiT$ compounds meet the first three conditions well (see Table SI in the Supplemental Material [29]). With respect to the last condition of tetragonal shear elastic constant $C'$, it is widely accepted as an effective parameter to predict the tendency of martensitic phase transition [33]. In general, the lower $C'$ corresponds to higher temperature of martensitic phase transition. Moreover, Zener anisotropy factor $(A)(= \frac{2C_{44}}{C_{11} - C_{12}} = \frac{C_{44}}{C'})$ was selected as another parameter to characterize phase stability [34]. Commonly, $A$ should be 1 for perfectly isotropic Heusler compounds. When $A$ deviates from 1, the cubic compounds become unstable and transform to low-symmetric martensitic phase [17]. For the current $Co_2NiT$ compounds, both $C'$ and $A$ at ground states were calculated and are shown in Fig. 4. Obviously, all $Co_2NiT$ compounds show negative $C'$ and corresponding $A$ (except $Co_2NiY$ due to its negative $C_{44}$). These values strongly indicate that martensitic phase transition can occur
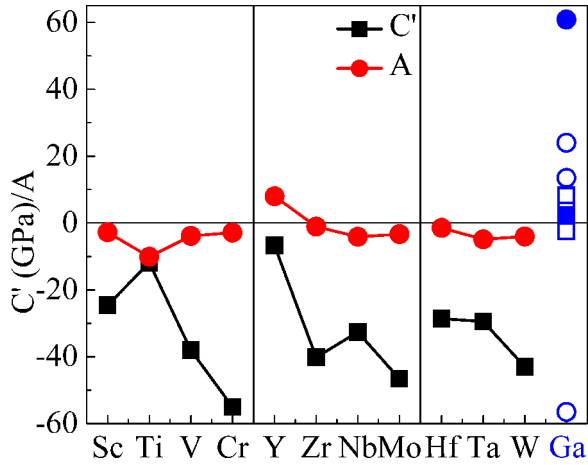
FIG. 4. Tetragonal shear elastic constant $C'$ (in GPa) and Zener anisotropy factor ($A$) of Co$_2$NiT ($T$ = Sc, Ti, V, Cr, Y, Zr, Nb, Mo, Hf, Ta, and W) compounds at ground states. To compare, $C'$ (open blue squares are from another theoretical study, solid ones are from this paper) and $A$ (open blue circles are from the other theoretical study, solid ones are from this paper) of Co$_2$NiGa are also collected and included herein. These cited values are from literature studies [30,31,36].



FIG. 5. The ductility parameters of Co$_2$NiT ($T$ = Sc, Ti, V, Cr, Y, Zr, Nb, Mo, Hf, Ta, W, and Ga) compounds: (a) Poisson's ratio, (b) $B/G_V$ ratio, (c) Cauchy's pressure (in GPa), and (d) Debye temperature (in K). For comparative analysis, parameters of conventional Co$_2$NiGa are also listed. Owing to the negative values of shear modulus ($G$), the Debye temperature and $B/G_v$ values of Co$_2$NiY are absent herein.

in them. Compared with well-studied Co$_2$NiGa [30,35,36], the lower $C'$ and $A$ in Co$_2$NiT compounds indicate higher martensitic phase transition temperature (see Fig. 4). Thus, high-temperature martensitic phase transition can be expected in all-$d$-metal Heusler compounds Co$_2$NiT.

One main objective of designing all-$d$-metal Heusler compounds is to improve inherent brittleness of conventional Heusler compounds, which results from directional $p$-$d$ covalent bonding between transition metals and main-group elements [17]. When main-group elements are fully replaced by transition metals in all-$d$-metal Heusler compounds, significant improvements of ductility can be expected due to the fundamental transformation of dominating interatomic bonding style from $p$-$d$ covalent hybridization to $d$-$d$ metallic bonding. For Co$_2$NiT compounds, their ductility could be evaluated from Poisson's ratio ($\upsilon$), the $B/G$ ratio, and Cauchy's pressure. Then the mechanism was discussed from the interatomic orbital hybridization style based on the calculated Debye temperature ($\Theta_D$) and electron localization function (ELF).

Based on the elastic constants of the single crystal listed in Table SI in the Supplemental Material [29], elastic moduli were derived by using the widely adopted Voigt-Reuss-Hill (VRH) approximation [37–39]. According to Voigt and Reuss approximations, the bulk and shear moduli of cubic compounds are deduced by using equations of $B_V = B_R = \frac{C_{11}+2C_{12}}{3}$, $G_V = \frac{C_{11}-C_{12}+3C_{44}}{5}$, and $G_R = \frac{5(C_{11}-C_{12})C_{44}}{4C_{44}+3(C_{11}-C_{12})}$. By using the VRH approximation, average bulk and shear moduli (i.e., $B_H = \frac{B_V+B_R}{2}$ and $G_H = \frac{G_V+G_R}{2}$) were obtained and listed in Table SI in the Supplemental Material [29]. Then Poisson's ratios were obtained by using $\nu = \frac{3B-2G}{2(3B+G)}$ [40]. Based on these parameters, first, the ductility of Co$_2$NiT can be judged from Poisson's ratio. The empirical critical Poisson's ratio to separate ductile and brittle materials is $\frac{1}{3}$ [41]. Commonly,

the higher the Poisson's ratio, the better the ductility. Figure 5(a) demonstrates that the Poisson's ratio ($\sim 0.30$) in conventional Co$_2$NiGa was the lowest and below the critical value, confirming its brittleness in nature. For Co$_2$NiT compounds, their Poisson's ratios are all higher than the critical value. This enhancement indicates that the improvement in the ductility of all-$d$-metal Heusler compounds Co$_2$NiT. Second, based on Pugh's [42] study, the $B/G$ ratio can work as another parameter to distinguish ductile materials from brittle ones. The threshold to separate ductile and brittle material is $\sim 1.75$. Materials with a $B/G$ ratio > 1.75 are generally considered ductile. Comparatively, a previous study on Heusler compounds indicates that the $B/G_V$ ratio based on $G_V$ can serve a better parameter [43]. Herein, $B/G_V$ ratios of Co$_2$NiT ($T$ = Sc, Ti, V, Cr, Zr, Nb, Mo, Hf, Ta, and W) compounds presented in Fig. 5(b) are all > 1.75 and higher than that of Co$_2$NiGa, further confirming improved ductility. For transition metal $T$ from the same period, Co$_2$NiT compounds with early transition metals possess higher $\upsilon$ and $B/G_V$, showing better ductility.

In solids, the inherent angular character of interatomic bonding is responsible for their mechanical performances. Physically, covalent bonding is characterized by an obvious angular feature and directional electronic distribution, which accounts for brittleness and consequently lower ductility in

solids. First, the property of interatomic bonding is described by using Cauchy's pressure ($C_p = C_{12} - C_{44}$). According to Pettifor, negative $C_p$ indicates more covalent characteristics, while the larger positive $C_p$ shows more metallic bonding characteristics [44]. Moreover, the larger the Cauchy's pressure, the more ductile the materials. Figure 5(c) (details in Table SI in the Supplemental Material [29]) shows that all Co$_2$NiT compounds possess positive $C_p$, and their values are higher than that of Co$_2$NiGa. It indicates more metallic bonding components and consequently more uniform electronic distribution in Co$_2$NiT compounds compared with conventional Co$_2$NiGa. It could be helpful to establish a nonangular metallic bonding characteristic and contribute to the improvement of ductility in Co$_2$NiT compounds. Second, interatomic bonding strength was compared by calculating Debye temperature ($\Theta_D$). In general, the higher $\Theta_D$ supports the stronger strength of covalent bonding in solids. In this paper, $\Theta_D$ of Co$_2$NiT compounds was evaluated by using the equation $\Theta_D = \frac{h}{k_B}[\frac{3q}{4\pi}\frac{N_A\rho}{M}]^{1/3}v_m$ [45], where $h$ and $K_B$ are the Planck and Boltzmann constants, respectively, $q$ is the number of atoms in each formula unit, $N_A$ is the Avogadro number, $M$ is the molecular weight per formula unit, and $\rho$ is the density. Here, $v_m(= [\frac{1}{3}(\frac{2}{v_t^3} + \frac{1}{v_l^3})]^{-1/3})$ is the average velocity, where $v_l(= \sqrt{(B + \frac{4}{3}G)\frac{1}{\rho}})$ and ($v_t(= \sqrt{\frac{G}{\rho}})$ are longitudinal and transverse sound velocities, respectively. The details of calculated $v_l$, $v_t$, $v_m$, and $\Theta_D$ are listed in Table SII in the Supplemental Material [29]. Compared with Co$_2$NiGa, all Co$_2$NiT compounds exhibit lower $\Theta_D$, as shown in Fig. 5(d). Thus, a weakened covalent hybridization level in Co$_2$NiT was revealed by lowered $\Theta_D$, which is consistent with the claim from Cauchy's pressure. To conclude, both Cauchy's pressure and the Debye temperature proved that the $d$-$d$ metallic bonding component in Co$_2$NiT compounds was enhanced and became dominant. This enhancement promoted more uniform distribution of electrons, which was found to be responsible for the improved ductility of Co$_2$NiT compounds. Comparatively, Co$_2$NiT compounds with early transition metal atoms exhibited relatively low $\Theta_D$, as shown in Fig. 5(d). It indicates their better ductility, which is in good agreement with the evaluation from Poisson's ratio and the $B/G_V$ ratio.

The calculation of ELF is a visual and qualitative strategy to reveal the distribution of electrons and the interatomic bonding characteristic in solids [46]. In this paper, the typical ELF distributions of conventional Co$_2$NiGa and representative Co$_2$NiTi in all-$d$-metal Heusler compounds were calculated, as shown in Figs. 6(a) and 6(b), respectively. In general, ELF = 1 indicates the highest level of electron accumulation, indicating a complete covalent bonding. When ELF = 0.5, the distribution of electrons is uniform, which corresponds to a metallic bonding. Values ranging from 0.5 to 1 indicate a transition from metallic bonding to covalent bonding. In stark contrast with Co$_2$NiTi, the electron accumulation level between Ga and its 1nn transition metal Co atoms in Co$_2$NiGa is higher. The ELF value is ~0.78, indicating stronger covalent hybridization. The interatomic coupling style illustrates the obvious directional mode. In contrast, the distribution of electrons in Co$_2$NiTi becomes much more uniform, as confirmed by the ELF value of 0.59.
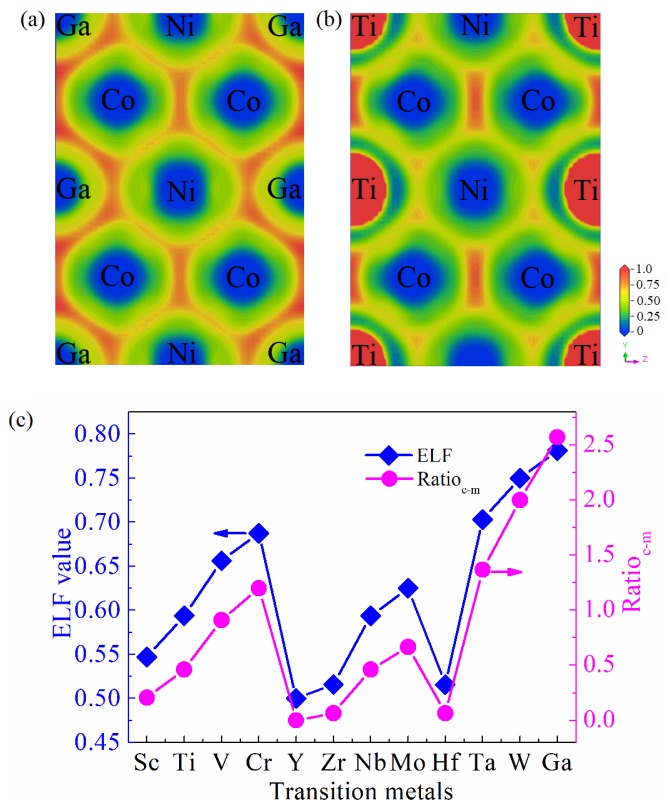


FIG. 6. (a) and (b) The typical electron localization function (ELF) on (110) plane in unit cell of conventional $L2_1$-type Heusler compound Co$_2$NiGa and isostructural Co$_2$NiTi all-$d$-metal Heusler compound, respectively. The reference bar on the bottom right corner indicates ELF value. The higher electron accumulation level between 1nn Co and Ga atom pairs in Co$_2$NiGa reveals stronger covalent hybridization strength. (c) The ELF value and covalent to metallic strength ratio of Co$_2$NiT ($T$ = Sc, Ti, V, Cr, Y, Zr, Nb, Mo, Hf, Ta, and W) compounds.

This result demonstrates a stronger metallic bonding characteristic in Co$_2$NiTi [47]. Comparatively, Co$_2$NiTi possesses better metallicity, which is responsible for the improved ductility. Similar values of ELF were observed in other Co$_2$NiT compounds, as presented in Fig. 6(c). Notably, all Co$_2$NiT compounds investigated in this paper show smaller values of ELF than that for Co$_2$NiGa. The substitution of transition metals for main-group element Ga is effective to tune the distribution of electrons and improve the ductile properties. Moreover, the Co$_2$NiT compounds with early transition metals show smaller values of ELF than those with late transition metals in the same period. Furthermore, ELF was adopted as a parameter to scale the covalent to metallic strength ratio in this paper. Based on the average interatomic ELF of involved compounds, the covalent-to-metallic strength ratio might be approximated as Ratio$_{c-m} = \frac{1}{1-ELF} - 2$, in which the ELF value ranges from 0.5 to 1. For a covalent bonding compound with ELF value ~1, the covalent-to-metallic strength ratio tends to be infinite. In ideal metallic bonding compounds, the covalent-to-metallic strength ratio is zero due to the ELF value of 0.5. Following this method, the covalent-to-metallic

strength ratios of $Co_2NiT$ all-$d$-metal Heusler compounds were theoretically obtained, and the corresponding results are shown in Fig. 6(c). Herein, for facilitating comparative analysis of chemical bonding, the color mapping values were set in the same range during the analysis of ELF. Then the ELF values were renormalized to be between 0 and 1. The results shown in Fig. 6(c) illustrate that the highest covalent-to-metallic strength ratio was obtained for $Co_2NiGa$, supporting its brittle nature. Comparatively, $Co_2NiT$ compounds show lower ratios. Moreover, the dependence of covalent-to-metallic strength ratios in $Co_2NiT$ compounds on transition metal atoms, as presented in Fig. 6(c), shows a similar change tendency to that of ELF. This consistency verified that the approximation method to evaluate the covalent-to-metallic strength ratio is feasible. Comparative analysis indicates that the covalent hybridization was weakened by the full replacement of transition metals for main-group elements. As a result, the increased metallicity results in the enhancement of ductile parameters of $Co_2NiT$ compounds, particularly in those with early transition metals, as shown in Fig. 5. Consequently, the above-calculated Cauchy's pressure, Debye temperature, ELF, and covalent-to-metallic strength ratio all indicate that the enhanced metallicity in $Co_2NiT$ compounds results in the increase in ductile performance.

Comparative analysis indicates that the metallic bonding component in $Co_2NiT$ compounds with early transition metals is higher. The smaller the number of valence electrons in $Co_2NiT$ compounds, the stronger the metallic bonding. Owing to the volume effect of the metallic bonding, $Co_2NiT$ compounds with early transition metals could prefer more close-packed structures. However, the changing trends of lattice parameters dependent on specific transition metals in Fig. 2(c) show that $Co_2NiT$ compounds with early transition metals possess greater lattice sizes, which can be attributed to the larger atomic radii. Thus, the current findings clearly indicate that the influence of the atomic radius on lattice size is overpowering and has a greater impact on the lattice size of all-$d$-metal Heusler compounds $Co_2NiT$.

Practically, in solids, metallic bonding can still be maintained when they undergo relative sliding of atomic layers and do not easily collapse even under certain external forces. Thus, excellent deformability could be expected in the ductile $Co_2NiT$ compounds. Compared with that in covalent compounds, the energy consumed to overcome bond distortion and breaking in metallic compounds is lowered. Consequently, the nucleation and propagation of dislocation become relatively easy. The higher density of dislocation is achieved in materials with real metallic bonding, which helps enhance the plastic performance in $d$-$d$ metallic-bonding-dominated $Co_2NiT$ compounds. Thus, tuning the interatomic bonding style can serve as an effective design scheme to explore ductile functional materials. This design scheme can provide more options for future theoretical and experimental studies.

### C. Electronic structures

For more comprehensive and in-depth understanding of the cubic phase stability of $Co_2NiT$ compounds, herein, the DOSs were calculated and shown in Fig. 7. For comparative analysis, the DOSs of conventional $Co_2NiGa$ in $L2_1$-type structures were also obtained, as shown in Fig. 7(1). All DOSs of $Co_2NiT$ compounds in this paper possess typical peak-and-valley characterized distribution near the Fermi level ($E_F$). In Heusler compounds, this type of DOS distribution arises from highly localized $d$ bands and van Hove singularities at the band edges of $d$ bands, in conjunction with a smooth shift of peaky DOS structure relative to the Fermi energy when valence electrons are added to the system. The tetragonal distortion via martensitic phase transformation is a favorable approach to remove the high DOSs, which makes the equivalent $k$ points in the cubic structure inequivalent. Moreover, the degeneracy of occupied states is lifted, and the bandwidth is broadened. All these changes can smoothen the peak-and-valley-like distribution of DOSs near $E_F$ and lower the energy of cubic phase. Commonly, this peak-and-valley-like DOS distribution served as the intuitive criterion to determine phase stability [48–50]. Thus, the occurrence of martensitic phase transition can be identified in $Co_2NiT$ compounds based on the peak-and-valley character of DOSs near $E_F$. Compared with $Co_2NiGa$, the deeper and more typical peak-and-valley-like DOS distribution in $Co_2NiT$ compounds indicates that their cubic structures are more unstable. Consequently, higher possibilities of martensitic phase transition can be expected in all-$d$-metal compounds $Co_2NiT$. Thus, they can serve as high-temperature martensitic phase transition materials. Current judgments on the phase stability of $Co_2NiT$ compounds agree with the evaluation from the elastic moduli presented in Fig. 4.

### D. Lattice dynamics properties

Phonon dispersion can serve as another parameter to scale the dynamic stability of these compounds. To further comprehend the phase stability of cubic $Co_2NiT$ compounds, phonon dispersions along the symmetry line at preferential crystal structures were calculated and shown in Fig. 8. For $Co_2NiT$ compounds, the most attracting characteristic is the softening of two transverse acoustic (TA) phonon modes along *G-X-W* directions. Obviously, all local minima at the *X* point of the Brillouin zone locate at imaginary frequencies range. Figure 8(1) illustrates that these minima dependent on specific atoms gradually become weaker with the increase of valence electrons of transition metals in each period. The occurrence of imaginary frequencies in phonon dispersions strongly reveals that cubic $Co_2NiT$ compounds are dynamically unstable to shear deformation corresponding to the eigenvector of TA modes. High-temperature martensitic phase transition can occur in them. Moreover, the more the valence electrons in transition metal atoms, the higher the possibility of martensitic phase transition, which is consistent with the judgment from elastic parameters and electronic structures.

The abovementioned results of elastic parameters, electronic structures, and lattice dynamics properties indicate that cubic $Co_2NiT$ is prone to martensitic phase transition at the high-temperature zone. Thus, the cubic phases could be observed only at high temperatures. At room temperature, the low-symmetric martensitic phases could be expected. Thus, further experiments are necessary to verify current theoretical predictions.

To further identify the physical origin of unstable phonon modes in $Co_2NiT$ compounds, representative partial phonon
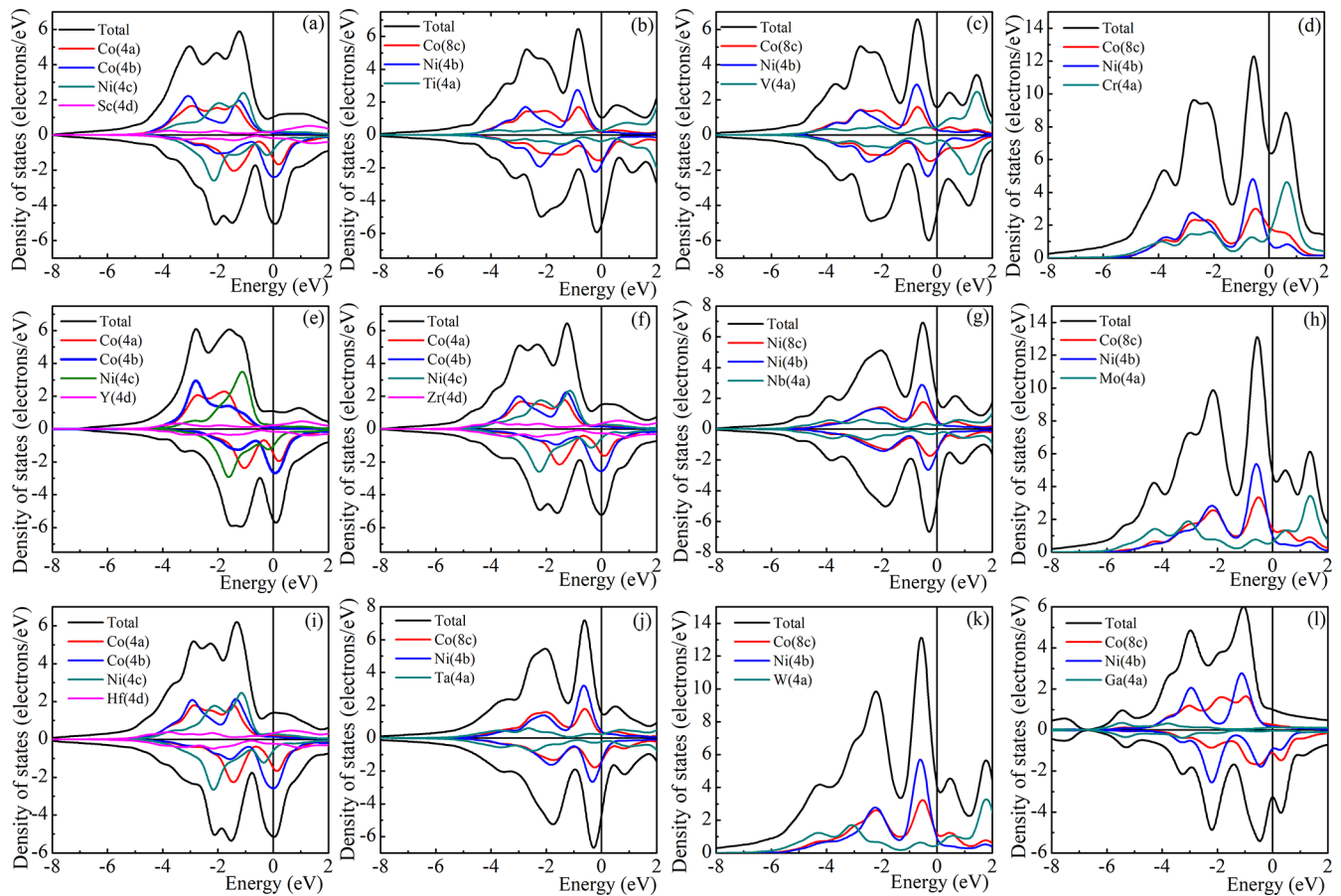
FIG. 7. (a)–(k) Calculated spin-projected density of states (DOS) plots of $Co_2NiT$ ($T$ = Sc, Ti, V, Cr, Y, Zr, Nb, Mo, Hf, Ta, and W) compounds. The total and partial DOSs for $d$ electrons of atoms on specific crystalline sites are included. The upper halves of each panel display the spin-up states. For nonmagnetic $Co_2NiCr$, $Co_2NiMo$, and $Co_2NiW$, only spin-up direction DOSs are shown here. (l) The DOS of $Co_2NiGa$ for comparative analysis.

DOSs of $Co_2NiHf$, $Co_2NiTa$, and $Co_2NiW$ were selected, as shown in Fig. 9. Normally, atomic mass determines the sequence of atomic contribution to phonon dispersions [51]. In general, lighter atoms dominate the high-frequency phonon modes and vice versa. Unusually, Figs. 9(a)–9(c) demonstrate that the lighter Co atoms dominate the medium-frequency phonon dispersions, which are below the optical modes of heavier Ni atoms. This inversion behavior acts via hybridization as a repulsive force on the acoustical modes, and it is also responsible for the occurrence of imaginary frequency phonon modes [51]. Consistent judgments about the cubic phase stability of $Co_2NiHf$, $Co_2NiTa$, and $Co_2NiW$ based on phonon dispersion and DOSs reveal strong interaction between electronic structure near $E_F$ and phonon dispersion, which brings about the Kohn anomaly. Thus, the martensitic phase transition in $Co_2NiT$ compounds could origin from the Kohn anomaly [52]. To further verify the abovementioned statements, precise experiments were suggested to reveal the mechanism of martensitic phase transition in $Co_2NiT$ compounds.

Figure 3 shows that $Co_2NiT$ all-$d$-metal Heusler compounds with B2- and A2-type structures exhibit higher energies than those with ordered cubic structures. As a result, disordered B2- and A2-type structures are less stable. When the disorder level increases, the transition from the parent

cubic phase to the low-symmetric martensitic phase should become considerably easier. Compared with that in ordered cubic structures, the atomic disorder in B2- and A2-type structures altered the structural symmetry and thus changed the Fermi surface [53]. Notably, the Kohn anomaly results from a specific geometry of the Fermi surface; therefore, the introduction of atomic disorder contributes to this singularity. Currently, it is computationally unfeasible to calculate phonons and investigate the Kohn anomaly in a supercell with random atomic disorders [54]. Therefore, undeniably, more advanced theoretical and experimental research is needed to gain a thorough grasp of the effect of atomic disorder on the Kohn anomaly, which will be pursued in the future.

### E. Correlation between magnetism and martensitic phase transition

For all-$d$-metal Heusler-type martensitic phase transition materials, the contribution of magnetism to phase stability deserves further systematic investigations. To identify the role of magnetism on martensitic phase transition in all-$d$-metal Heusler compounds $Co_2NiT$, the magnetic moments were calculated and presented in Fig. 10 (see details in Table I). For $Co_2NiT$ compounds, the magnetic states vary from strong or weak FIM in $Co_2NiT$ with early transition metals
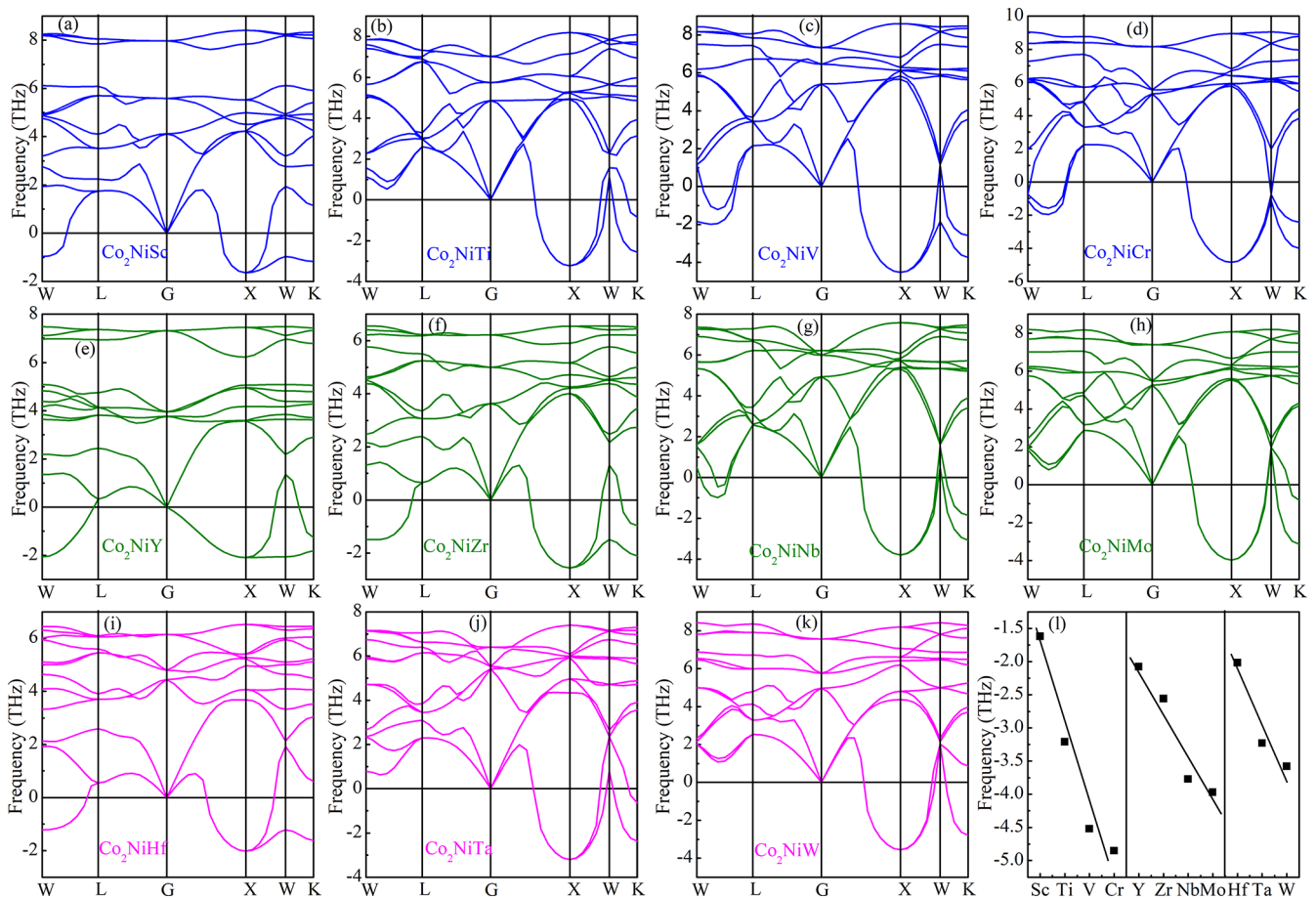
FIG. 8. (a)–(k) The phonon dispersions of $Co_2NiT$ ($T$ = Sc, Ti, V, Cr, Y, Zr, Nb, Mo, Hf, Ta, and W) compounds. Imaginary frequencies in negative frequency range indicate unstable phonon modes. The high-symmetry $q$ point path in the Brillouin zone was selected as $W(0.5,0.25,0.75) \rightarrow L(0.5,0.5,0.5) \rightarrow G(0,0,0) \rightarrow X(0.5,0,0.5) \rightarrow W(0.5,0.25,0.75) \rightarrow K(0.375,0.375,0.75)$. (l) Imaginary frequency values at the $X$ point dependent on specific transition metal atoms.

($T$ = Sc, Ti, V, Y, Zr, Nb, Hf, and Ta) to NM states in $Co_2NiT$ with late transition metals ($T$ = Cr, Mo, and W). The above-

calculated elastic moduli, electronic structures, and phonon dispersions confirmed that martensitic phase transition could occur in all $Co_2NiT$ compounds. Comprehensive analysis of these theoretical observations indicates that magnetism is not the necessary condition for the occurrence of martensitic
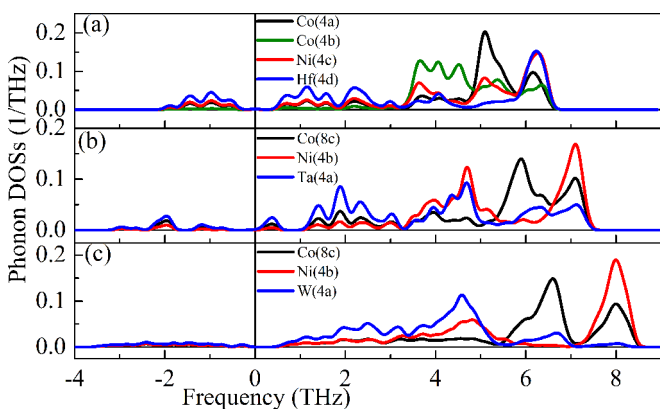


FIG. 9. (a)–(c) Site projected phonon densities of states (DOS) of $Co_2NiHf$, $Co_2NiTa$, and $Co_2NiW$, respectively. The phonon dispersions dominated by lighter Co atom abnormally lie below the optical modes of the heavier Ni atoms. This anomalous behavior could act via hybridization as a repulsive force on the transverse acoustical modes.
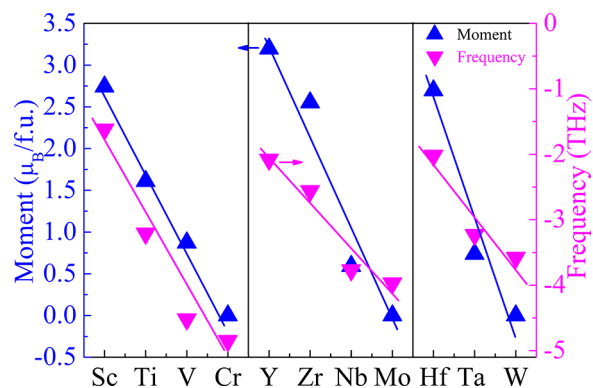


FIG. 10. Magnetic moments dependence of transition metals in all-$d$-metal Heusler compounds $Co_2NiT$ ($T$ = Sc, Ti, V, Cr, Y, Zr, Nb, Mo, Hf, Ta, and W). To facilitate comparison, imaginary frequency values at the $X$ point in phonon dispersions are listed herein.

TABLE I. The calculated magnetic moments for all-$d$-metal Heusler compounds Co$_2$NiT ($T$ = Sc, Ti, V, Cr, Y, Zr, Nb, Mo, Hf, Ta, and W) at theoretical equilibrium states. The atomic moment (in $\mu_B$) on specific sites of 4$a$, 4$b$, 4$c$, and 4$d$ in Hg$_2$CuTi-type structure and 8$c$, 4$a$, and 4$b$ in Cu$_2$MnAl-type structure, and their total moments (in $\mu_B$/f.u.) are both listed herein. For comparative analysis, the magnetic moments of Co$_2$NiGa are also included.

| Compounds | 4$a$/8$c$ | 4$b$/4$b$ | 4$c$/8$c$ | 4$d$/4$a$ | Total | Ref. |
|---|---|---|---|---|---|---|
| Co$_2$NiSc | 1.26 | 1.54 | 0.06 | −0.12 | 2.74 | This paper |
| Co$_2$NiTi | 0.78 | 0.36 | 0.78 | −0.34 | 1.61 | This paper |
| Co$_2$NiV | 0.62 | 0.16 | 0.62 | −0.52 | 0.87 | This paper |
| Co$_2$NiCr | 0 | 0 | 0 | 0 | 0 | This paper |
| Co$_2$NiY | 1.46 | 1.72 | 0.1 | −0.08 | 3.20 | This paper |
| Co$_2$NiZr | 1.16 | 1.54 | −0.02 | −0.12 | 2.55 | This paper |
| Co$_2$NiNb | 0.3 | 0.12 | 0.3 | −0.1 | 0.59 | This paper |
| Co$_2$NiMo | 0 | 0 | 0 | 0 | 0 | This paper |
| Co$_2$NiHf | 1.22 | 1.58 | −0.02 | −0.1 | 2.70 | This paper |
| Co$_2$NiTa | 0.46 | 0.1 | 0.46 | −0.28 | 0.74 | This paper |
| Co$_2$NiW | 0 | 0 | 0 | 0 | 0 | This paper |
| Co$_2$NiGa | 1.14 | 0.55 | 1.14 | −0.05 | 2.77 | This paper |
| | 1.143 | | 1.143 | | | [55] |
| | 1.262 | | 1.262 | | | [30] |
| | 0.935 | 0.474 | 0.935 | −0.067 | 2.27 | [56] |
| | | | | | 2.67 | [57] |



FIG. 11. The energy difference between austenitic and martensitic phases under various magnetic configurations. NMA and FIMA denote nonmagnetic and ferrimagnetic austenite, respectively. FIMM stands for ferrimagnetic martensite.

phase transition. When it comes to transition metal atoms from the same period, as shown in Fig. 10, the moments of Co$_2$NiT compounds decrease linearly with the increase of valence electrons. Moreover, simultaneous decrease in imaginary frequency values at the $X$ point in phonon dispersions indicates the increased possibility of martensitic phase transition. These results indicate that the loss or absence of magnetism decreases the phase stability of cubic Co$_2$NiT compounds.

To further explore the role of the magnetic moment on phase stability in Co$_2$NiT ($T$ = Sc, Ti, V, Y, Zr, Nb, Hf, and Ta) compounds, the energy differences among FIM austenite (FIMA), NM austenite (NMA), and FIM martensite (FIMM) were calculated and shown in Fig. 11. Herein, the NM state was the nonpolarized configuration. Since the ground states of Co$_2$NiT ($T$ = Sc, Ti, V, Y, Zr, Nb, Hf, and Ta) compounds belong to the FIM state, the energy under FM states could not be obtained, although the parallel arrangement of atomic magnetic moments was initially set during the calculations. Figure 11 exhibits that the energy difference $\Delta E$ (= $E_{FIMA}$ − $E_{FIMM}$) is positive, which indicates that the FIMM phase is more stable. This energy difference provides the driving force for the occurrence of martensitic phase transition. When the magnetic states of Co$_2$NiT ($T$ = Sc, Ti, V, Y, Zr, Nb, Hf, and Ta) compounds become NM, the energy difference between NMA and FIMM phases, i.e., $\Delta E$ (= $E_{NMA}$ − $E_{FIMM}$), becomes larger. The austenite phases are less stable. Herein, the loss of magnetic moment resulted in larger energy differences, which consequently led to easy driving of the martensitic phase transition. Obviously, martensitic phase transition was found to be closely correlated with magnetism. Comparatively, it can be concluded that, although magnetism is not the necessary condition for the occurrence of martensitic phase
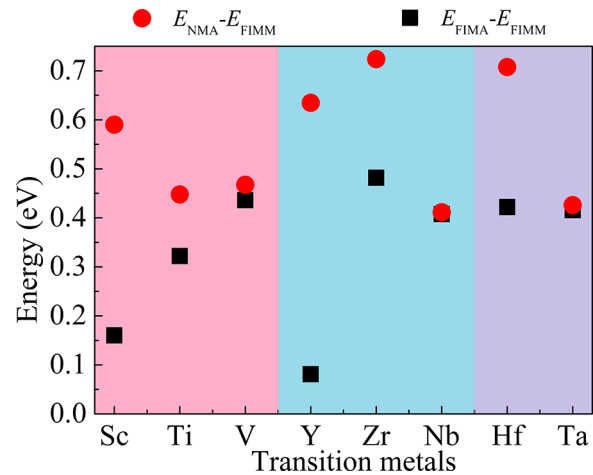
transition, the annihilation of magnetic moments destabilizes the cubic structure. Consequently, any modulating methods to weaken magnetic moments such as application of external pressure or chemical pressure via adjusting atomic content serves as an effective way to tune martensitic phase transition in Co$_2$NiT compounds.

Coincidentally, the very recent studies on Ni$_2$Mn$T$ ($T$ = transition metals) Heusler compounds and Cu-doped Ni$_2$MnGa conventional Heusler compounds also revealed a stronger correlation between magnetism and martensitic phase transition [58,59]. These observed results indicate that the contribution from magnetism cannot be ignored when discussing free energy and corresponding phase stability [60,61]. At finite temperature, the contribution from magnetic moment to free energy is proportional to magnetic entropy, i.e., $S^{mag} = R \ln(\beta + 1) = R \sum_i c_i \ln(\beta_i + 1)$ [61], where $R$ is the gas constant, $\beta_i$ denotes the local magnetic moments of atom $i$, and $c_i$ is the concentration of atom $i$. Obviously, the bigger the moments, the larger the magnetic entropy. Thus, in compounds with a strong magnetic moment, the contribution from $-TS^{mag}$ could result in lower free energy and thus stabilize the structure. However, a weak magnetic moment is expected to result in relatively high-energy states and can drive the transformation of compounds to more stable states. Under this circumstance, martensitic phase transition from high- to low-symmetric phase is prone to occur. At finite temperature, the magnetic moment plays an important role on the free energy and phase stability.

### F. Quasivolume-preserving martensitic phase transition in Co$_2$NiT ($T$ = Ti and V) compounds

To reveal the characteristic of the martensitic phase in Co$_2$NiT compounds, $c/a$ ratio-dependent total energy at different volumes was calculated, and the corresponding results are shown in Fig. 12(a), considering Co$_2$NiTi as a representative example. These calculations were carried out in a large volume change and $c/a$ span allowing for the possible martensitic phase transition. Figure 12(a) exhibits the
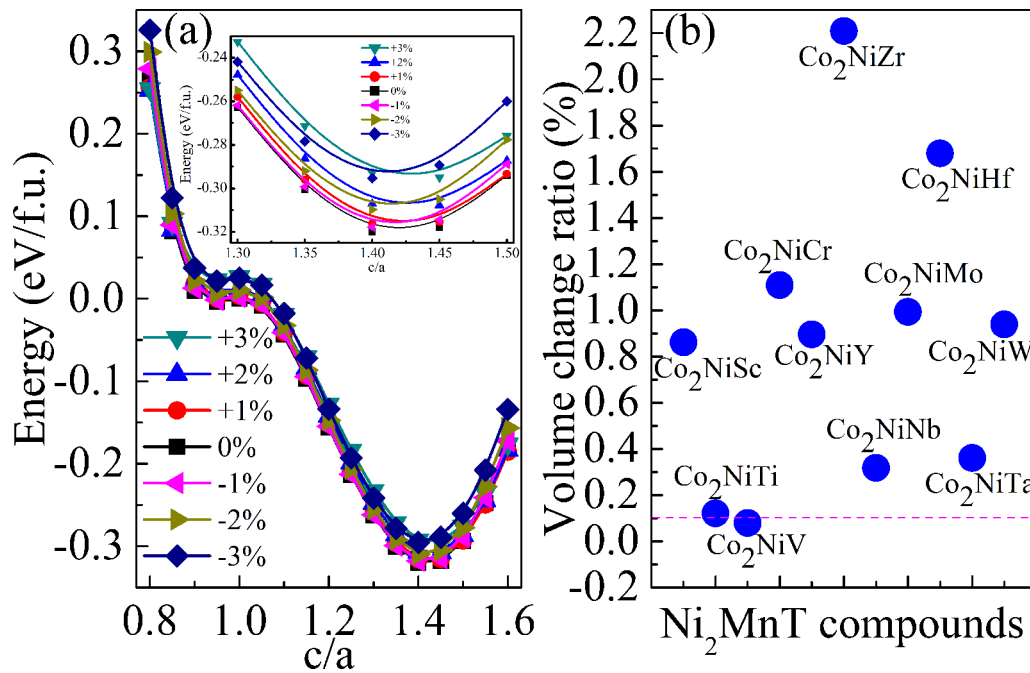
FIG. 12. (a) Calculated total energy (eV f.u.$^{-1}$) of $Co_2NiTi$ compound in $L2_1$ structure as a function of the $c/a$ ratio, considering the total energy of cubic $Co_2NiTi$ at ground state as reference. Herein, the volume change ratio of 0, $\pm 1$, $\pm 2$, and $\pm 3\%$ are considered. Inset shows the enlarged span around the global minimum with the $c/a$ ratio changing from 1.30 to 1.50. (b) The volume change ratio between cubic phase and martensitic phase in all-$d$-metal Heusler compounds $Co_2NiT$ ($T$ = Sc, Ti, V, Cr, Y, Zr, Nb, Mo, Hf, Ta, and W). The lower values indicate that the volume change ratios during martensitic phase transition are smaller.

presence of two obvious local minima, which lie in the low and high $c/a$ ratio span, respectively. The two local minima indicate that possible martensitic phase transition can occur in $Co_2NiTi$. The calculated $c/a$ ratios of tetragonal phases are $\sim 0.90$ and 1.42, respectively. They are like the theoretical values of other all-$d$-metal Heusler compounds [13,62,63]. Comparatively, the tetragonal phase with $c/a = 1.42$ is stable in energy, while the tetragonal phase with $c/a = 0.9$ is metastable. When considering the effect of volume, it is observed that the martensitic phase prefers the volume of cubic $Co_2NiTi$ at the ground state. During the martensitic phase transition, smaller or negligible volume change occurred in $Co_2NiTi$. For precise investigation of the volume changes during the martensitic phase transition, geometric optimizations were carried out for the martensitic phase of $Co_2NiT$. The calculated data of volume change ratios during the transition from cubic to tetragonal phase were collected and presented in Fig. 12(b). For the abovementioned $Co_2NiTi$ compound, the theoretical volume change ratio during the martensitic phase transition was found to be $\sim 0.12\%$. Moreover, the volume change ratio was found to be closely related to the hysteresis of martensitic phase transition. Experimentally, in $Mn_2NiGa$, a volume variation of 0.64% was observed, which was accompanied by a thermal hysteresis of 50 K [64]. However, in the $Ni_{2.2}Mn_{0.8}Ga$ compound, the volume change ratio was 0.12%. The observed hysteresis width during the martensitic phase transition was only 5 K [65]. In general, the smaller the volume change during martensitic phase transition, the narrower the hysteresis width. The reversibility of phase transition could be better, which could benefit the future technical applications.

The volume change ratios of other $Co_2NiT$ compounds were also calculated and presented in Fig. 12(b). Comparatively, it was found that $Co_2NiV$ possessed the smallest volume change ratio (0.0791%). The small volume change between cubic austenite and tetragonal martensitic phases may be ascribed to the fact that the two phases are compatible, or an exact interface is formed between them. The occurrence of a geometric compatibility condition for transition from austenite to martensite phases helped to significantly lower the hysteresis [65]. Thus, the theoretically expected narrow hysteresis width during phase transition could endow high-temperature martensitic phase transition compounds $Ni_2MnTi$ and $Ni_2MnV$ with more extensive application prospects.

## IV. CONCLUSIONS

Martensitic phase transition, ductile properties, and magnetism of all-$d$-metal Heusler compounds $Co_2NiT$ were systematically investigated by DFT calculations from elastic constants, electronic structure, and lattice dynamics. First, in contrast to the atomic preferential occupation rule in the conventional Heusler family, all-$d$-metal Heusler compounds $Co_2NiT$ with late transition metal atoms ($T$ = Ti, V, Cr, Nb, Mo, Ta, and W) prefer $L2_1$-type structure rather than $Hg_2CuTi$-type structure. Furthermore, different from $p$-$d$ covalent hybridization-dominated conventional Heusler compounds, inherent atomic radii become the decisive factor in determining the lattice sizes of all-$d$-metal Heusler compounds $Co_2NiT$. Second, in $Co_2NiT$ compounds, the coupling between electronic peak-and-valley-like DOS near the Fermi level and negative frequency of TA phonon modes brings out

the Kohn anomaly, which induces high-temperature martensitic phase transitions. Comparatively, although magnetism is not the necessary condition for the occurrence of martensitic phase transition, the loss or absence of magnetism can destabilize the cubic structure. Thus, magnetism can serve as another effective parameter to tune martensitic phase transition in all-$d$-metal Heusler compounds $Co_2NiT$. Third, compared with $p$-$d$ covalent hybridization-controlled conventional Heusler compounds, the $d$-$d$ metallic bonding in all-$d$-metal Heusler compounds $Co_2NiT$ helps boost more uniform distribution of electrons and consequently results in enhancing ductility. This fundamental improvement of ductility endows $Co_2NiT$ compounds with outstanding mechanical performance. Finally, the smaller volume change ratios in $Co_2NiTi$ and $Co_2NiV$ compounds enable them to be more promising and attractive as high-temperature martensitic phase transition materials. It is speculated that this paper can be conducive for in-depth understanding of the mechanism of martensitic phase transition, the physical origin of improved ductility, and the role of magnetism on phase stability in all-$d$-metal Heusler compounds, which can help in exploring high-temperature martensitic phase transition materials with excellent performance.

[1] R. J. Ma, Z. Y. Zhang, K. W. Tong, D. Huber, R. Kornbluh, Y. S. Ju, and Q. B. Pei, Highly efficient electrocaloric cooling with electrostatic actuation, Science **357**, 1130 (2017).

[2] B. Li, Y. Kawakita, S. Ohira-Kawamura, T. Sugahara, H. Wang, J. Wang, Y. Chen, S. I. Kawaguchi, S. Kawaguchi, K. Ohara *et al.*, Colossal barocaloric effects in plastic crystals, Nature (London) **567**, 506 (2019).

[3] V. Franco, J. S. Blázquez, J. J. Ipus, J. Y. Law, L. M. Moreno-Ramírez, and A. Conde, Magnetocaloric effect: From materials research to refrigeration devices, Prog. Mater. Sci. **93**, 112 (2018).

[4] L. Manosa and A. Planes, Materials with giant mechanocaloric effects: Cooling by strength, Adv. Mater. **29**, 1603607 (2017).

[5] X. Moya, E. Defay, V. Heine, and N. D. Mathur, Too cool to work, Nat. Phys. **11**, 202 (2015).

[6] T. Gottschall, A. Gràcia-Condal, M. Fries, A. Taubel, L. Pfeuffer, L. Mañosa, A. Planes, K. P. Skokov, and O. Gutfleisch, A multicaloric cooling cycle that exploits thermal hysteresis, Nat. Mater. **17**, 929 (2018).

[7] J. Liu, T. Gottschall, K. P. Skokov, J. D. Moore, and O. Gutfleisch, Giant magnetocaloric effect driven by structural transitions, Nat. Mater. **11**, 620 (2012).

[8] Y. Shen, Z. Wei, W. Sun, Y. Zhang, E. Liu, and J. Liu, Large elastocaloric effect in directionally solidified all-$d$-metal Heusler metamagnetic shape memory alloys, Acta Mater. **188**, 677 (2020).

[9] Z. Y. Wei, E. K. Liu, J. H. Chen, Y. Li, G. D. Liu, H. Z. Luo, X. K. Xi, H. W. Zhang, W. H. Wang, and G. H. Wu, Realization of multifunctional shape-memory ferromagnets in all-$d$-metal Heusler phases, Appl. Phys. Lett. **107**, 022406 (2015).

[10] Z. Y. Wei, E. K. Liu, Y. Li, X. L. Han, Z. W. Du, H. Z. Luo, G. D. Liu, X. K. Xi, H. W. Zhang, W. H. Wang *et al.*, Magnetostructural martensitic transformations with large volume changes and magneto-strains in all-$d$-metal Heusler alloys, Appl. Phys. Lett. **109**, 071904 (2016).

[11] D. Cong, W. Xiong, A. Planes, Y. Ren, L. Mañosa, P. Cao, Z. Nie, X. Sun, Z. Yang, X. Hong *et al.*, Colossal elastocaloric effect in ferroelastic Ni-Mn-Ti alloys, Phys. Rev. Lett. **122**, 255703 (2019).

[12] G. Li, E. Liu, W. Wang, and G. Wu, Theoretical investigations on elastic properties, phase stability, and magnetism in $Ni_2Mn$-based all-$d$-metal Heusler compounds, Phys. Rev. B **107**, 134440 (2023).

[13] Y. Han, M. Wu, Y. Feng, Z. Cheng, T. Lin, T. Yang, R. Khenata, and X. Wang, Competition between cubic and tetragonal phases in all-$d$-metal Heusler alloys, $X_{2-x}Mn_{1+x}V$ ($X$ = Pd, Ni, Pt, Ag, Au, Ir, Co; $x$ = 1, 0): A new potential direction of the Heusler family, IUCrJ **6**, 465 (2019).

[14] H.-L. Yan, L.-D. Wang, H.-X. Liu, X.-M. Huang, N. Jia, Z.-B. Li, B. Yang, Y.-D. Zhang, C. Esling, X. Zhao *et al.*, Giant elastocaloric effect and exceptional mechanical properties in an all-$d$-metal Ni–Mn–Ti alloy: Experimental and *ab-initio* studies, Mater. Des. **184**, 108180 (2019).

[15] J. H. N. van Vucht, Influence of radius ratio on the structure of intermetallic compounds of the $AB_3$ type, J. Less-Common Met. **11**, 308 (1966).

[16] T. J. Burch, T. Litrenta, and J. I. Budnick, Hyperfine studies of site occupation in ternary systems, Phys. Rev. Lett. **33**, 421 (1974).

[17] G. Li, E. Liu, G. Liu, W. Wang, and G. Wu, Density functional theory investigation on lattice dynamics, elastic properties and origin of vanished magnetism in Heusler compounds CoMnVZ ($Z$ = Al, Ga), Chin. Phys. B **30**, 083103 (2021).

[18] D. Vanderbilt, Soft self-consistent pseudopotentials in a generalized eigenvalue formalism, Phys. Rev. B **41**, 7892 (1990).

[19] J. P. Perdew, K. Burke, and M. Ernzerhof, Generalized gradient approximation made simple, Phys. Rev. Lett. **77**, 3865 (1996).

[20] H. Akai, Fast Korringa-Kohn-Rostoker coherent potential approximation and its application to FCC Ni-Fe systems, J. Phys.: Condens. Matter **1**, 8045 (1989).

[21] H. Akai, Ferromagnetism and its stability in the diluted magnetic semiconductor (In, Mn)As, Phys. Rev. Lett. **81**, 3002 (1998).

[22] J. G. Tan, Z. H. Liu, Y. J. Zhang, G. T. Li, H. G. Zhang, G. D. Liu, and X. Q. Ma, Site preference and tetragonal distortion of Heusler alloy Mn-Ni-V, Results Phys. **12**, 1182 (2019).

[23] https://www.materialsproject.org.

[24] Z. H. Liu, M. Zhang, Y. T. Cui, Y. Q. Zhou, W. H. Wang, G. H. Wu, X. X. Zhang, and G. Xiao, Martensitic transformation and

shape memory effect in ferromagnetic Heusler alloy $Ni_2FeGa$, Appl. Phys. Lett. **82**, 424 (2003).

[25] T. Graf, C. Felser, and S. S. P. Parkin, Simple rules for the understanding of Heusler compounds, Prog. Solid State Chem. **39**, 1 (2011).

[26] G. J. Li, E. K. Liu, H. G. Zhang, J. F. Qian, H. W. Zhang, J. L. Chen, W. H. Wang, and G. H. Wu, Unusual lattice constant changes and tunable magnetic moment compensation in $Mn_{50-x}Co_{25}Ga_{25+x}$ alloys, Appl. Phys. Lett. **101**, 102402 (2012).

[27] G. J. Li, E. K. Liu, H. G. Zhang, Y. J. Zhang, J. L. Chen, W. H. Wang, H. W. Zhang, G. H. Wu, and S. Y. Yu, Phase diagram, ferromagnetic martensitic transformation and magnetoresponsive properties of Fe-doped MnCoGe alloys, J. Magn. Magn. Mater. **332**, 146 (2013).

[28] G. J. Li, E. K. Liu, H. G. Zhang, Y. J. Zhang, G. Z. Xu, H. Z. Luo, H. W. Zhang, W. H. Wang, and G. H. Wu, Role of covalent hybridization in the martensitic structure and magnetic properties of shape-memory alloys: The case of $Ni_{50}Mn_{5+x}Ga_{35-x}Cu_{10}$, Appl. Phys. Lett. **102**, 062407 (2013).

[29] See Supplemental Material at http://link.aps.org/supplemental/10.1103/PhysRevMaterials.7.104411 for the calculated elastic constants $C_{ij}$ and shear modulus $G$ (in GPa), longitudinal velocity, transverse velocity and average velocity (in m/s), and the Debye temperature (in K) for all-$d$-metal Heusler compounds $Co_2NiT$ ($T$ = Sc, Ti, V, Cr, Y, Zr, Nb, Mo, Hf, Ta and W).

[30] R. Arróyave, A. Junkaew, A. Chivukula, S. Bajaj, C. Y. Yao, and A. Garay, Investigation of the structural stability of $Co_2NiGa$ shape memory alloys via *ab initio* methods, Acta Mater. **58**, 5220 (2010).

[31] A. Talapatra, R. Arróyave, P. Entel, I. Valencia-Jaime, and A. H. Romero, Stability analysis of the martensitic phase transformation in $Co_2NiGa$ Heusler alloy, Phys. Rev. B **92**, 054107 (2015).

[32] F. Mouhat and F. X. Coudert, Necessary and sufficient elastic stability conditions in various crystal systems, Phys. Rev. B **90**, 224104 (2014).

[33] C.-M. Li, H.-B. Luo, Q.-M. Hu, R. Yang, B. Johansson, and L. Vitos, First-principles investigation of the composition dependent properties of $Ni_{2+x}Mn_{1-x}Ga$ shape-memory alloys, Phys. Rev. B **82**, 024201 (2010).

[34] C. Zener, *Elasticity and Anelasticity of Metals* (University of Chicago, Chicago, 1948), p. 21.

[35] E. Dogan, I. Karaman, N. Singh, A. Chivukula, H. S. Thawabi, and R. Arroyave, The effect of electronic and magnetic valences on the martensitic transformation of CoNiGa shape memory alloys, Acta Mater. **60**, 3545 (2012).

[36] J. Bai, D. Liu, R. Huang, Z. Zhang, Y. Yang, J. Gu, H. Yan, X. Zhao, and L. Zuo, Phase stability, magnetic and elastic properties of $Co_2NiGa$ alloy: A first-principles calculation, Mater. Today Commun. **22**, 100810 (2020).

[37] W. Voigt, Ueber die Beziehung zwischen den beiden Elasticitätsconstanten isotroper Körper, Ann. Phys. **274**, 573 (1889).

[38] A. Reuss, Berechnung der Fließgrenze von Mischkristallen auf Grund der Plastizitätsbedingung für Einkristalle, Z. Ang. Math. Mech. **9**, 49 (1929).

[39] R. Hill, The elastic behaviour of a crystalline aggregate, Proc. Phys. Soc. Sect. A **65**, 349 (1952).

[40] S. C. Wu, G. H. Fecher, S. S. Naghavi, and C. Felser, Elastic properties and stability of Heusler compounds: Cubic $Co_2YZ$ compounds with $L2_1$ structure, J. Appl. Phys. **125**, 082523 (2019).

[41] I. N. Frantsevich, F. F. Voronov, and S. A. Bokuta, *Elastic Constants and Elastic Moduli of Metals and Insulators Handbook* (Naukova Dumka, Kiev, 1983).

[42] S. F. Pugh, Relations between the elastic moduli and the plastic properties of polycrystalline pure metals, Philos. Mag. **45**, 823 (1954).

[43] S. Ghosh and S. Ghosh, Role of composition, site ordering, and magnetic structure for the structural stability of off-stoichiometric $Ni_2MnSb$ alloys with excess Ni and Mn, Phys. Rev. B **99**, 064112 (2019).

[44] D. G. Pettifor, Theoretical predictions of structure and related properties of intermetallics, Mater. Sci. Tech. **8**, 345 (1992).

[45] O. L. Anderson, A simplified method for calculating the Debye temperature from elastic constants, J. Phys. Chem. Solids **24**, 909 (1963).

[46] B. Silvi and A. Savin, Classification of chemical bonds based on topological analysis of electron localization functions, Nature (London) **371**, 683 (1994).

[47] S. H. Zhang, Q. Wang, Y. Kawazoe, and P. Jena, Three-dimensional metallic boron nitride, J. Am. Chem. Soc. **135**, 18216 (2013).

[48] J. Winterlik, S. Chadov, A. Gupta, V. Alijani, T. Gasi, K. Filsinger, B. Balke, G. H. Fecher, C. A. Jenkins, F. Casper *et al.*, Design scheme of new tetragonal Heusler compounds for spin-transfer torque applications and its experimental realization, Adv. Mater. **24**, 6283 (2012).

[49] L. Wollmann, S. Chadov, J. Kübler, and C. Felser, Magnetism in tetragonal manganese-rich Heusler compounds, Phys. Rev. B **92**, 064417 (2015).

[50] S. V. Faleev, Y. Ferrante, J. Jeong, M. G. Samant, B. Jones, and S. S. P. Parkin, Origin of the tetragonal ground state of Heusler compounds, Phys. Rev. Appl. **7**, 034022 (2017).

[51] P. Entel, V. D. Buchelnikov, V. V. Khovailo, A. T. Zayak, W. A. Adeagbo, M. E. Gruner, H. C. Herper, and E. F. Wassermann, Modelling the phase diagram of magnetic shape memory Heusler alloys, J. Phys. D: Appl. Phys. **39**, 865 (2006).

[52] C. Bungaro, K. M. Rabe, and A. D. Corso, First-principles study of lattice instabilities in ferromagnetic $Ni_2MnGa$, Phys. Rev. B **68**, 134104 (2003).

[53] O. N. Miroshkina, B. Eggert, J. Lill, B. Beckmann, D. Koch, M. Y. Hu, T. Lojewski, S. Rauls, F. Scheibel, A. Taubel *et al.*, Impact of magnetic and antisite disorder on the vibrational densities of states in $Ni_2MnSn$ Heusler alloys, Phys. Rev. B **106**, 214302 (2022).

[54] M. Ghim and S.-H. Jhi, Kohn anomalies in topological insulator thin films: First-principles study, J. Phys.: Condens. Matter **34**, 265002 (2022).

[55] N. Singh, E. Dogan, I. Karaman, and R. Arroyave, Effect of configurational order on the magnetic characteristics of Co-Ni-Ga ferromagnetic shape memory alloys, Phys. Rev. B **84**, 184201 (2011).

[56] E. Olivos, A. L. Miranda, N. Singh, R. Arroyave, and A. H. Romero, Spin excitations in $Co_2NiGa$ under pressure from a theoretical approach, Ann. Phys. **524**, 212 (2012).

[57] M. Siewert, M. E. Gruner, A. Dannenberg, A. Hucht, S. M. Shapiro, G. Xu, D. L. Schlagel, T. A. Lograsso, and P. Entel, Electronic structure and lattice dynamics of the magnetic shape-memory alloy $Co_2NiGa$, Phys. Rev. B **82**, 064420 (2010).

[58] G. Li, L. Xu, Z. Ding, and Z. Cao, Magnetism-dependent martensitic phase transition in $Ni_2Mn$-based all-$d$-metal Heusler compounds, Appl. Phys. Lett. **123**, 022401 (2023).

[59] G. Li, L. Xu, and Z. Cao, A unified physical mechanism for martensitic phase transition and ductility in Ni–Mn-based ferromagnetic shape memory alloys: The case of Cu-doped $Ni_2MnGa$, J. Mater. Chem. C **11**, 6173 (2023).

[60] F. Körmann, T. Hickel, and J. Neugebauer, Influence of magnetic excitations on the phase stability of metals and steels, Curr. Opin. Solid State Mater. Sci. **20**, 77 (2016).

[61] H. İ. Sözen, T. Hickel, and J. Neugebauer, Impact of magnetism on the phase stability of rare-earth based hard magnetic materials, Calphad **68**, 101731 (2020).

[62] M. Wu, F. Zhou, R. Khenata, M. Kuang, and X. Wang, Phase transition and electronic structures of all-$d$-metal Heusler-type $X_2MnTi$ compounds ($X$ = Pd, Pt, Ag, Au, Cu, and Ni), Front. Chem. **8**, 546947 (2020).

[63] G. Li, E. Liu, and G. Wu, $d$-$d$ hybridization controlled large-volume-change martensitic phase transition in Ni-Mn-Ti-based all-$d$-metal Heusler compounds, J. Alloy Compd. **923**, 166369 (2022).

[64] G. D. Liu, J. L. Chen, Z. H. Liu, X. F. Dai, G. H. Wu, B. Zhang, and X. X. Zhang, Martensitic transformation and shape memory effect in a ferromagnetic shape memory alloy: $Mn_2NiGa$, Appl. Phys. Lett. **87**, 262504 (2005).

[65] P. Devi, M. Ghorbani Zavareh, C. S. Mejía, K. Hofmann, B. Albert, C. Felser, M. Nicklas, and S. Singh, Reversible adiabatic temperature change in the shape memory Heusler alloy $Ni_{2.2}Mn_{0.8}Ga$: An effect of structural compatibility, Phys. Rev. Mater. **2**, 122401(R) (2018).